Atomic contributions to friction and load for tip–self-assembled monolayers interactions

M. Todd Knippenberg,[1] Paul T. Mikulski,[1] Brett I. Dunlap,[2] and Judith A. Harrison[1]
[1]*Departments of Chemistry and Physics, United States Naval Academy, Annapolis, Maryland 21402, USA*
[2]*Theoretical Chemistry Section, Code 6189, Naval Research Laboratory, Washington D.C. 20375, USA*
(Received 23 July 2008; revised manuscript received 20 October 2008; published 3 December 2008)

Scanning force microscopies (SFM) are being routinely used to examine the mechanical and tribological properties of materials with the goal of obtaining information, such as Young's Moduli and shear strengths from the experimental data [Unertl, J. Vac. Sci. Technol. A **17**, 1779 (1999)]. Analysis of data obtained from an SFM experiment typically requires the use of continuum mechanics models to extract materials properties. When applying these models care must be taken to ensure that the experimental conditions meet the requirements of the model being applied. For example, despite many successful applications of the Johnson-Kendall-Roberts (JKR) model to SFM data, it does not take into account the presence of a compliant layer on the sample surface. Recent AFM experiments that examined the friction of self-assembled monolayers (SAMs) have confirmed that friction versus load data cannot be fit by the JKR model. The authors suggest that the penetration of the SAM by the tip gives rise to an additional contribution to friction due to "plowing" [Flater *et al.*, Langmuir **23**, 9242 (2007)]. Herein, molecular-dynamics simulations are used to study atomic contact forces between a spherical tip in sliding contact with a SAM. These simulations show that different regions around the tip contribute in unanticipated ways to the total friction between the tip and the monolayer and allow for the number and location of monolayer atoms contributing friction to be determined. The use of atomic contact forces within the monolayer, instead of forces on the rigid tip layers, allows for the contributions to friction force (and load) to be deconvoluted into forces that resist (repel) and assist (attract) tip motion. The findings presented here yield insight into the AFM experiments of SAMs and may have important consequences for the adaptation of continuum contact models for the contact between a sphere and surface where penetration into the sample is possible.

DOI: 10.1103/PhysRevB.78.235409 PACS number(s): 68.35.Af, 46.70.−p, 62.20.Qp

I. INTRODUCTION

Single-asperity contact measurements have proven to be a very useful tool for examining mechanical properties[1,2] and nanotribology at well-defined interfaces.[3–18] The AFM is the most widely used technique for these studies because forces and displacements of the tip and sample can be accurately measured.[18] In addition, the AFM has been used extensively to examine the nanotribological properties of self-assembled monolayers (SAMs) because SAMs provide a flexible, convenient, and simple system with which to tailor the interfacial properties of metals, metal oxides, and semiconductors.[19,20] In addition to being promising candidates for boundary-layer lubricants in nanoscale devices, such as microelectromechanical systems (MEMS),[21] SAMs are model systems for the study of lubrication at the molecular level because they form well-packed monolayers.[8,19,22] Over the past several years the frictional properties of SAMs as a function of chain length,[9,23–25] packing density (order),[14,17,26,27] fluorination,[16,17,28,29] and terminal group[10,23,30] have been studied extensively using the AFM. While early work was primarily focused on the nanometer-scale friction of alkanethiols on Au[9,13,14,26,31–34] and alkylsilanes on Si,[25,27,35–38] the friction of other types of monolayers has been recently examined.[39]

The extraction of materials properties, such as Young's Modulus and interfacial shear strength, from AFM data relies upon the use of contact mechanics models. The application of these models must be done with careful attention being paid to the underlying assumptions and limits of each model. Models that apply to isotropic elastic contacts, such as Derjaguin-Muller-Toporov (DMT) and Johnson-Kendall-Roberts (JKR),[40] have been used successfully to interpret AFM data in cases were interfacial friction is the dominant contribution to friction.[41–51] It should be noted, however, that the addition of a compliant layer, such as a SAM, to the substrate complicates the analysis of data obtained with the AFM. In these cases, it is not expected that the DMT or JKR models would be applicable and recent experiments[27,39,52] have demonstrated that this is the case.

Several contact models have appeared in the literature that are designed to model compliant layers on hard substrates under different circumstances.[53–58] For example, Johnson and Sridhar[53] extended JKR theory to include a compliant elastic coating on a compliant substrate while neglecting friction between the indentor and the surface. Viscoelastic effects have been incorporated into JKR theory so that the modulus of elastomeric films could be studied.[56] Lin *et al.*[58] modeled the compliant layer as a Neo-Hookean layer. Finally, Reedy[57] developed a model for the contact of a rigid spherical indentor contacting a thin linear elastic coating to a rigid substrate. In that model, the ratio of the layer thickness divided by the radius of the sphere is assumed to be much less than one. Despite the existence of these models, there are only a few cases of their successful application to the AFM data of deformable materials.[59–61] This may be due, in part, to the existence of addition contributions to friction present in SAMs which are not present in other systems. Recent experiments have hypothesized that the friction of SAMs was the sum of the interfacial friction and a plowing

term, where plowing arises from the compression and displacement of molecules by the tip.[27,39]

Molecular-dynamics (MD) simulations have been used extensively to examine the structure and friction of SAMs. A significant number of early simulations examined the structure, mechanical, and tribological properties of alkanethiol monolayers on Au (Refs. 62 and 63) and model organic monolayers.[64] Much of this work has been discussed in a recent review.[65] More recently, the mechanical and tribological properties of alkylsilane monolayers[66–71] and monolayers composed of hydrocarbon chains[72–80] have been investigated extensively using MD. These studies have examined the effects of packing density,[69,74,77] sliding speed,[70] fluorine and -OH termination,[67,68] the odd-even effect,[78] sliding direction,[65,74,77] chain length,[65,71,73] and polymerization of the monolayer chains on friction,[76] as well as the periodic response of the monolayer to sliding.[75] Much of the work to date has utilized the simulation geometry that places two infinite plates in sliding contact. There are comparitively few studies that have utilized a finite-sized tip and an infinite plate geometry.[62,65,71,72] In this work, MD simulations were used to examine the atomic-scale friction between a rigid spherical indentor and a model SAM composed of alkane chains on a hard substrate. In particular, the way in which individual monolayer atoms support the load and contribute to friction was examined via the use of contact forces. The results presented here, combined with previous simulations that have examined the validity of continuum mechanics models at the nanometer scale,[81,82] may prove helpful in the application, and development, of contact mechanics to systems with compliant layers.

II. METHOD

To mimic an AFM friction study, a finite-sized rigid spherical tip was placed in sliding contact with a model SAM. The monolayer was composed of 270 *n*-alkane chains with 14 carbon atoms $[-(CH_2)_{13}-CH_3]$ attached to a diamond (111) surface in the (2×2) arrangment. This arrangement has been used in our previous studies[72,74,77,80] and yields a packing density that is similar to alkanethiols on Au(111).[19,20] The plane that contained the monolayer was 75.4 Å by 78.4 Å and periodic boundary conditions were applied. The diamond substrate contained three layers of carbon atoms. The bottom layer of diamond was held rigid, and a Berendsen thermostat was applied to the remaining diamond layers to maintain the average temperature of the system at 290 K.[83] The spherical tip was composed of 720 carbon atoms, had a radius of ~13 Å, and was composed entirely of five-membered or six-membered rings so that its shape resembled that of a 720-atom fullerene (Fig. 1).[84]

The adaptive intermolecular reactive empirical bond-order (AIREBO)[85] potential was used to calculate the forces within the MD simulations. The AIREBO potential contains terms to model covalent bonding, based on the second-generation reactive empirical bond-order (REBO) potential,[86] torsional terms, and intermolecular terms. The addition of these terms to the REBO potential significantly increases the computational time for simulations that use the AIREBO potential compared to the REBO potential. With this in mind, the simulation system was carefully designed to balance the dimensions of the plane containing the monolayer with the radius of the spherical tip. The thickness of the diamond substrate, to which the SAM is attached, was designed to be the minimum number of layers that could be used to support the SAM and apply the thermostat, while not adversely influencing the simulation results. Newton's equations of motion were integrated using a time step of 0.25 fs.

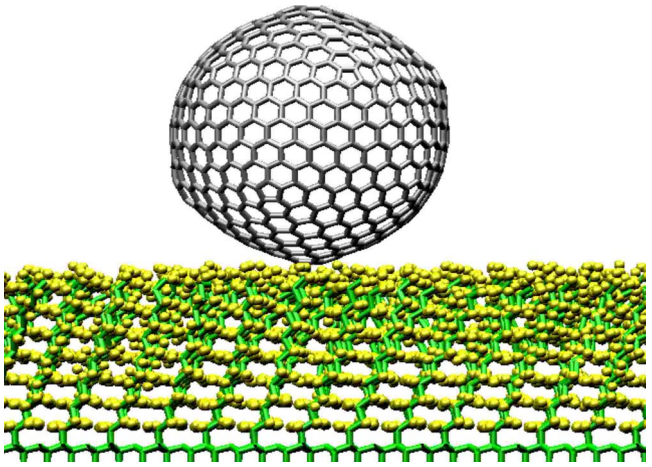

FIG. 1. (Color online) Snapshot of the MD simulation system under a 0 nN load. The spherical fullerene tip (gray) is located above the monolayer composed of C_{14} alkane chains, which is attached to diamond (yellow and green). Hydrogen atoms of the SAM are shown as spheres and the carbon backbones of the chains and the diamond are shown in wireframe. Sliding is accomplished by moving the spherical tip from left to right.

Once the temperature and potential energy of the monolayer and diamond were equilibrated, the tip was introduced above the monolayer. The entire system was then re-equilibrated under the target load while sliding. While several loads were examined, the contact-force distribtutions are qualitatively similar for all nonzero applied loads. Therefore, results for 0 nN and the representative load of 10 nN are discussed in detail. During the course of this equilibration, a feedback loop computes the forces between tip and the monolayer atoms,[77] raising or lowering the tip to arrive at the target load. After the system was equilibrated, the tip was moved at a constant velocity of 87.1 m/s in the direction of the chain *cant*. This velocity is based on the unit cell of the monolayer, which is 8.71 Å in length. While this sliding velocity is much higher than the μm/s speeds that are used in AFM experiments, this speed is consistent with previous simulation sliding speeds.[77,78,80] Moreover, the friction of alkylsilane monolayers[66,67] was shown to be invariant in the range of computationally accessible sliding speeds (0.2–100 m/s).

III. RESULTS

The average friction on the spherical tip as a function of load when it is in sliding contact with the SAM is shown in Fig. 2. As the load on the tip is increased, the friction in-

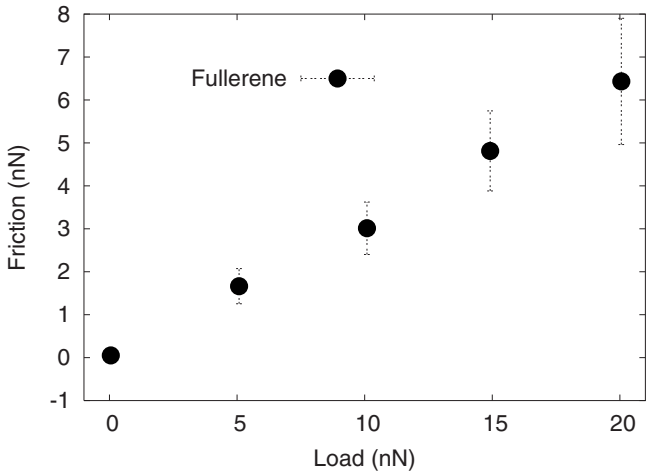

FIG. 2. Average friction on the fullerene tip as a function of load when the tip is in sliding contact with a monolayer composed of C_{14} alkane chains as shown in Fig. 1.

creases in a linear fashion. The quantity that is most directly connected with what is measured in an AFM experiment is the net force on the rigid tip atoms shown in Fig. 2. It can be difficult to relate this net force on the rigid atoms to events and structural changes that take place at the interface during sliding. Recently, it has been shown that there is a negligible difference between rigid-layer and all-atom forces exerted on either the tip, or the sample, when averaging over time scales which are much larger than those associated with the bonded atom oscillations.[78,80] The all-atom forces are composed of average contact forces on individual monolayer atoms. The average contact force is defined as the force on a given atom due to only the tip atoms averaged over 2000 time steps or 500 fs. The sliding simulation is 260 ps; thus, the average contact force on each monolayer atom is output 520 times for postsimulation analysis. These average contact forces can be analyzed in creative ways to yield insight into the way in which structural features influence friction force.[78,80] The main advantage of using the average contact forces is that the forces on individual monolayer atoms normal to, and tangential to, the sliding interface, and the role they play in supporting the load and friction, can be investigated. In particular, the contributions each atom makes to the total force that resists the forward motion of the tip can be separated from the contributions that push the tip in the sliding direction. Loading forces on each monolayer atom can also be separated into repulsive and attractive contributions. For simplicity, hereafter, contact force will refer to the average contact force on each monolayer atom.

The distribution of contact forces in the *loading direction on* the monolayer atoms is shown as a function of distance from the center of the spherical fullerene tip in Fig. 3. These distributions are calculated by dividing the plane that contains the monolayer into d_y segments, or bins, that are 0.1 Å wide. The contact forces in the loading direction (F_z) on all the SAM atoms in a d_y bin are summed. The total force in each bin is divided by the total bin width (dF_z/d_y). All time frames are included in this distribution. (All contact-force distributions presented here are calculated in this way.) Thus,

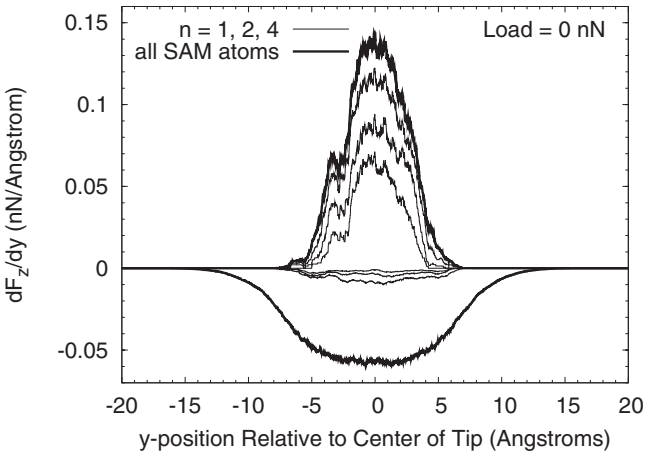

FIG. 3. The sum of average contact forces on the monolayer atoms in the *loading* direction in a d_y slice of the monolayer (dF_z/d_y) as a function of distance from a fixed atom at the bottom center of the fullerene. Repelling (+) and attractive (–) forces are tracked (and binned) separately. The heavy black lines with the largest minima and maxima represent the contribution to load from all monolayer atoms. On average, ten and 452 atoms contribute to the repelling and the attracting all-atom distributions, respectively. Integration of the area enclosed by this all-atom curve recovers the total applied load on the tip (0 nN). Contributions to load from a subset of the monolayer atoms that bear the highest load are shown with thinner black lines, beginning with the atom ($n=1$) that bears the highest load. The numbers of atoms used to construct these distributions, i.e., $n=1$, $n=2$, increases with the height of the distribution. The line closest to zero dF_z/d_y, or $n=1$, corresponds to the single atom with the largest load.

integration of the area enclosed by the distribution constructed using all the monolayer atoms shown in Fig. 3 yields the total applied load on the tip. Positive and negative values of dF_z/d_y correspond to forces that repel and those that attract the tip, respectively. When the total applied load on the tip is 0 nN, both the attractive and repulsive regions of the contact-force distribution are approximately symmetric about the center of the tip ($y=0$). However, the part of the distribution that contains forces that repel the tip contains a shoulder centered near $y \approx -3.0$ Å and perhaps a second near $y \approx -6.0$ Å. The origin of these shoulders can be determined by separating the contact forces on the hydrogen monolayer atoms from the forces on the carbon atoms. The distribution of repelling forces created from forces on the carbon atoms (Fig. 4) is symmetric about zero and does not contain a marked shoulder. In contrast, the distribution created from the monolayer hydrogen atoms contains a shoulder and is nearly identical to the all-atom distribution shown in Fig. 3. It is also clear from examination of the distributions in Fig. 4 that, due to their proximity to the tip, the monolayer hydrogen atoms are responsible for the majority of the repelling forces while the carbon atoms repel the tip to only a small extent. Because the carbon atoms are farther from the tip, the scale of the attractive forces is larger than the repelling forces on these atoms.

Distributions such as the all-atom distribution shown in Fig. 3 can also be constructed using a subset of monolayer atoms. For example, the subset composed of the four (n

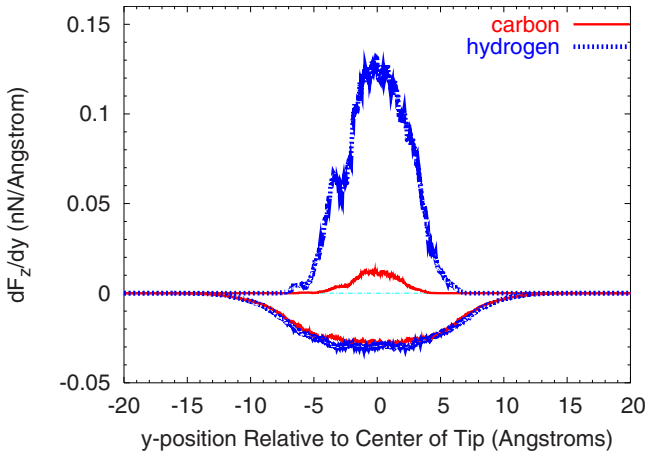

FIG. 4. (Color online) The contact forces in the *loading* direction on all monolayer atoms in a d_y slice of the monolayer (dF_z/d_y) as a function of distance from a fixed atom at the bottom center of the fullerene. Repulsive (+) and attractive (–) contributions to the contact force from monolayer hydrogen (dashed blue line) and carbon (solid red line) atoms are binned separately. Integration of the area enclosed by both of these distributions yields the total applied load on the tip (0 nN).

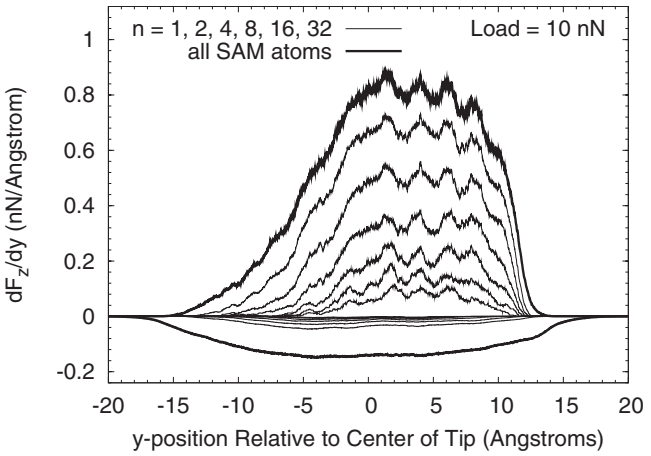

FIG. 5. The distribution of average contact forces in the *loading* direction on the monolayer atoms as a function of distance from a fixed atom at the bottom center of the fullerene. Repelling (+) and attractive (–) forces are tracked (and binned) separately. The darkest line represents the contribution to load from all monolayer atoms. On average, 101 and 1219 atoms contribute to the repelling and the attracting all-atom distributions, respectively. Contributions to load from the highest load-bearing atoms are shown with thinner lines, beginning with the highest load-bearing atom ($n=1$) as the line closest to 0 dF_z/d_y.

=4) monolayer atoms with the largest normal forces can be used to calculate a distribution (Fig. 3). This distribution is calculated in the same way as the all-atom distribution except that for each time frame only the four monolayer atoms with the largest contact forces in the loading direction are included. In the region of the distribution composed of repelling forces, the data constructed from this subset of atoms are nearly identical to the all-atom distribution. In other words, at any given moment in time when the total load is 0 nN, four monolayer atoms are responsible for the majority of the repelling forces on the tip, while many more atoms need to be included to approach the all-atom attractive portion of the distribution. In fact, an average of only ten atoms are needed to construct the all-atom distribution in the repelling region at this load, while 452 atoms are included on average in the attractive region of the all-atom distribution.

Because the tip is finite sized, the application of load causes the fullerene tip to penentrate into the monolayer. This penetration into the monolayer results in marked changes in the distribution of contact forces in the loading direction for all nonzero values of applied load. All the distributions at nonzero values of applied load possess the same qualitative features. The distribution when the load is 10 nN is shown in Fig. 5. The attractive portion of this distribution is still approximately symmetric about the center of the tip, although not as symmetric as it was at 0 nN. In contrast, the portion of the distribution constructed from repelling forces is skewed in the sliding direction (toward $+y$ values). Because the contact force on the monolayer atoms is calculated while sliding and the tip is "plowing" through the monolayer at all positive nonzero loads, the chains in front of the tip are in close proximity to the tip and are being pushed against other chains in front of the tip. In other words, the interaction of the hydrogen atoms on the chains with the tip is largely responsible for the repelling force, and a distribution constructed using contact forces on only the hydrogen atoms is nearly identical to the all-atom distribution shown in Fig. 5. The carbon atoms that comprise the backbone of the monolayer chains are effectively "shielded" from interaction with the tip by the presence of the attached hydrogen atoms. Thus, the scale of the repelling forces on the chain-carbon atoms is smaller than the scale of the attracting forces.

By separating the contributions to the total load in this way it is clear that when the tip is under a positive nonzero load, the repelling forces are the largest contributors to the load on the tip. Nonbonded interactions in the AIREBO potential are modeled using a Lennard-Jones (LJ) potential. Because the tip is finite, the application of load causes the fullerene tip to penentrate into the monolayer. This effect has also been observed in other simulations that model a finite-sized tip interacting with a SAM.[65,72] The magnitude of the forces in the repulsive portion of this potential change more dramatically with small changes in distance than in the attractive region. As a result, the disparity between the magnitude of the repelling and attracting forces increases as the load is increased. It is also possible to construct the loading-force distribution using a fixed number of atoms which make the greatest contribution to the load (Fig. 5). At this nonzero load, of the 101 atoms in repulsive contact, a subset of 32 atoms, which are all hydrogen atoms, makeup a significant fraction of the repulsive forces, while many more atoms (1219 on average) would be needed to encompass the attractive portion of the distribution. In fact, 33 monolayer atoms with nonzero contact forces in the loading direction account for 96% of the applied load.

The distribution of contact forces on the monolayer atoms in the sliding direction are shown in Figs. 6 and 7. Positive and negative force values are plotted as separate distributions

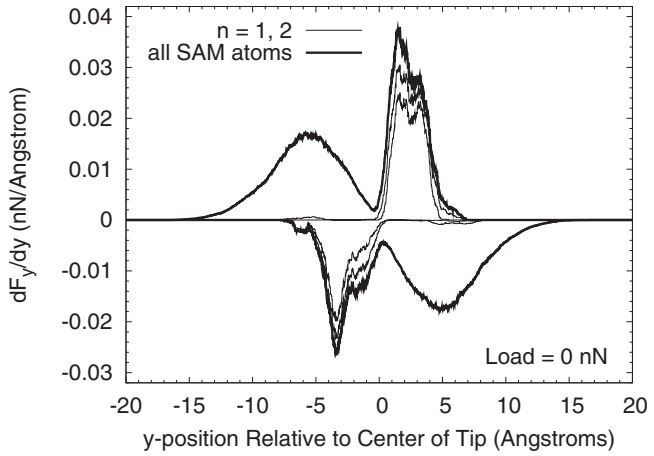

FIG. 6. The distribution of average contact forces in the *sliding* direction on all the monolayer atoms as a function of distance from a fixed atom at the bottom center of the fullerene. In these distributions, resisting (+) and pushing (−) forces are traced (and binned) separately. On average, 228 and 234 atoms contribute to the resisting and the pushing all-atom distributions, respectively.

and correspond to forces that resist tip motion and those that "push" the tip in the sliding direction, respectively. When the contact forces are plotted as in Figs. 6 and 7, the net friction force is obtained by taking the sum of the area under the all-atom resisting and pushing distributions. Thinner lines in Figs. 6 and 7 corrrespond to distributions constructed using a subset of monolayer atoms with the largest contact forces.

Both the 0 nN and 10 nN sliding-force distributions contain four regions: a region of resisting (+) and pushing (−) forces in front of the tip and regions of positive and negative forces behind the tip. Atoms in front of the tip (+y values) naturally oppose the motion of the tip moving past them. When these atoms are in close proximity to the tip, they interact via the hard-wall portion of the LJ potential. This hard-wall interaction gives rise to the (+) values of contact

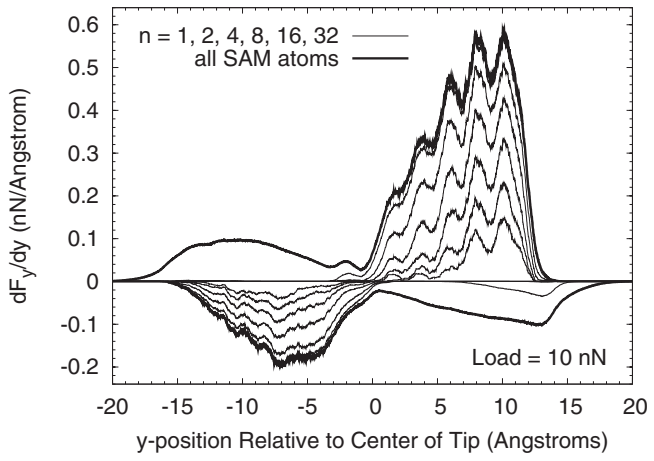

FIG. 7. The distribution of average contact forces in the *sliding* direction on all the monolayer atoms as a function of distance from a fixed atom at the bottom center of the fullerene. In these distributions, resisting (+) and pushing (−) forces are traced (and binned) separately. On average, 641 and 679 atoms contribute to the resisting and the pushing all-atom distributions, respectively.

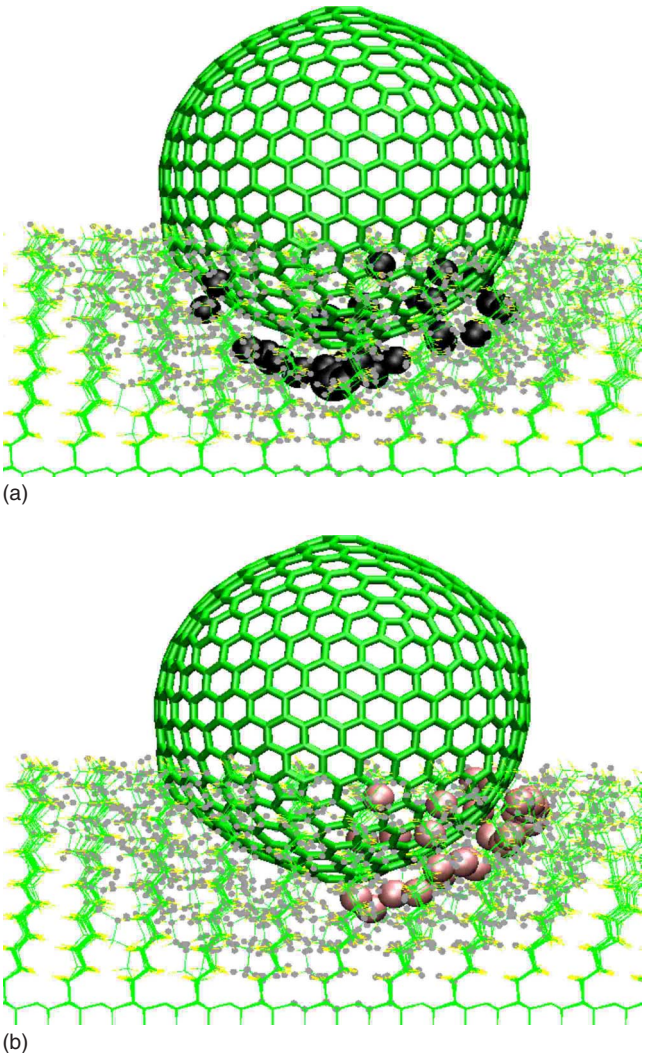

FIG. 8. (Color online) The simulation system viewed from the side under a 10-nN load. The tip moves from left to right to simulate sliding. The 32 monolayer atoms with the largest (a) repelling and (b) resisting forces are represented by black and pink spheres, respectively. Dots represent atoms with nonzero values of contact force. The remaining tip and the monolayer atoms are shown in wireframe.

force in front of the tip (+y) in both the 0 nN and 10 nN sliding-force distributions (Figs. 6 and 7). Because the application of load causes the tip to penetrate into the monolayer, it must plow through the monolayer, passing over some chains and pushing others out of the way. The monolayer atoms in this region of the distribution with the largest resisting forces are shown in Fig. 8(b) for the case when the load is 10 nN. It is clear from this figure that the tip is "plowing" through the monolayer. As a result, the magnitude of the contact forces in front of the tip are much larger at 10 nN (Fig. 7) than the magnitude of that type of force at 0 nN (Fig. 6). In fact, as the load is increased, the magnitude of the forces in this region of the histogram grows accordingly.

When the tip passes over, or by, the monolayer atoms, the tip and the monolayer still interact via the hard-wall portion of the LJ; however, the sign of the force changes to (−). As a result, atoms behind the tip (−y values) are able to extert a

force on the tip in the sliding direction that aids the motion of the tip. These regions of (−) force behind the tip are apparent in both the 0 nN and the 10 nN distributions (Figs. 6 and 7). Because this force is "pushing" the tip in the sliding direction, it reduces the net friction force experienced by the tip. The scale of the forces in the two regions of the contact-force distribution that arise from the hard-wall portion of the LJ potential are larger than the scale of the forces in the remaining two regions of the distributions discussed below. This disparity increases with the application of load. It follows that these types of interactions are the largest contributors to the net friction force experienced by the tip. It should also be noted that when the load on the tip is 10 nN (Fig. 7), there is a pronounced difference in the scale of the resisting forces (+) in front of the tip compared to the scale of pushing forces (−) behind the tip. This is not the case at 0 nN.

As with the loading distributions, it is possible to construct distributions of forces in the sliding direction using a subset of monolayer atoms with the largest contact forces. These distributions are represented by the series of lines labeled $n=1,2,4$, etc. in Figs. 6 and 7. As more and more atoms with nonzero contact forces are considered, the shape of these partial-atom distributions approaches that of the distribution constructed using all the monolayer atoms. For example, the distribution constructed from the 32 atoms with the largest resisting forces in front of the tip is very similiar to the all-atom distribution (Fig. 7). This is also the case for the pushing (−) forces behind the tip. In other words, when the load on the tip is 10 nN, at any point in the sliding simulation, there are only 32 atoms that contribute significantly to the total contact force that resists tip motion in front of the tip and that pushes the tip from behind in the sliding direction. In fact, these 32 atoms account for 88% of the total friction. It should be noted, however, that at any given time, a given atom is *either* pushing or resisting the tip. All of these atoms are hydrogen atoms attached to the carbon atoms within the alkane chains, and the majority of these atoms differ from the atoms that support the largest fraction of the load [Figs. 8(a) and 8(b)]. The "zigzag" nature of the carbon backbone of each chain places every other -CH_2- group in an orientation that gives particularly strong resisting contact with the tip at nonzero loads during plowing. Referring to the terminal -CH_3- group of each C_{14} chain as the 14th group and labeling the -CH_2- groups 13, 12, 11,…, then it is groups 13, 11, and 9 that are primarily responsible for the five well-defined shoulders (Fig. 7) in the resisting-force distributions as these groups interact at particular "catching" regions associated with the structure of the fullerene tip.

In contrast, at 0 nN the tip is not plowing through the monolayer (Fig. 1). In this case, the shape of the all-atom distributions can be approximated by including far fewer monolayer atoms in the distributions (Figs. 6). The atoms that contribute most to the resisting portion of the distribution in front of the tip and the pushing distribution behind the tip are hydrogen atoms directly below the tip.

The remaining two regions of the sliding-force distributions correspond to the resisting forces (+) behind the tip ($-y$) and to the pushing forces (−) in front of the tip ($+y$). Both of these types of forces arise from interactions in the attractive region of the LJ potential. When the tip has passed by a monolayer atom, the distance between the monolayer atom and the tip increases so that the interaction is governed by the attractive region of the LJ. Because the force is attractive, the monolayer atom resists the motion of the tip moving away from it. These forces correspond to the resisting (+) forces at negative values of tip position in the distribution. In front of the tip, there are monolayer atoms that are far enough in front of the tip to be in the attractive region of the potential. This attractive force "pulls" the tip in the sliding direction and is, therefore, classified as a pushing force at positive values of tip position. These two regions are apparent in both the 0 nN and the 10 nN distributions (Figs. 6 and 7). These two regions of the distribution are direct consequences of the finite size of tip and are not apparent in contact-force distributions when an infinite amorphous carbon counterface is in sliding contact with a monolayer[77,80] or when a lubricant was squeezed between a tip and a surface governed by purely repulsive interactions.[87]

In contrast to the regions of the distributions that arise from interactions with the hard wall of the LJ, the regions that arise from attractive interactions involve large numbers of atoms. For example, examination of Fig. 7 reveals that the distribution constructed from the 32 atoms with the largest forces does not overlap with the all-atom force distribution. In other words, due to the long-range nature of the attractive portion of the LJ slightly more atoms contribute to these portions of the distributions. However, because the attractive portion of the LJ is weaker than the repulsive region, the scale of the forces in these two regions of the distributions is much smaller.

IV. DISCUSSION

Single-asperity friction forces obtained with an AFM are proportional to the true contact area if the friction is dominated by interfacial friction, the shear strength of the interface is constant, and the contact pairs are isotropic linearly elastic materials.[41,43,45,50,51,88,89] In these cases, the friction varies with load in a nonlinear way. In contrast, the friction of alkanephosphonic acid SAMs varied linearly with load.[39] Two separate hypotheses were put forth to explain this linear dependence:[39] (1) the shear strength of the interface is pressure dependent or (2) friction is dominated by molecular plowing. In that work, the plowing model was hypothesized to lead to deformation of molecules localized under the tip and led to little deformation of the SAM outside the contact. Thus, the tip must plow through the monolayer during sliding. Plowing was also proposed as a significant contributor to the friction of octadecyltrichlorosilane monolayers.[27] The simulations presented here yield linear friction versus load data and the mechanism of sliding is consistent with the proposed plowing mechanism described by Brukman *et al.*[39] That is, deformation is localized to the region in close proximity to the tip [Figs. 8(a) and 8(b)]. Localized deformation of the monolayer chains in the indentation region has also been observed in simulations that used single-wall[72,90] and double-wall[65] carbon nanotubes to indent alkane monolayers.

A detailed examination of the contact forces (i.e., the force between each monolayer atom and the tip) in the load-

ing and sliding directions between a spherical tip and the model SAM have been carried out. Both the loading and friction forces at the interface were deconvoluted into their positive and negative components and examined as a function of position relative to the tip. This type of analysis allowed for the distribution of forces at the contacting interface to be elucidated. The contact forces during sliding can be separated into four categories. In front of the tip, there are (+) forces that resist tip motion and forces (−) that pull the tip in the sliding direction. Behind the tip, there are (−) forces that push tip in the sliding direction and forces (+) that resist the movement of the tip away from monolayer atoms. As the tip penetrates into the SAM (i.e., the load increases), the scale of the forces (+) that resist tip motion in front of the tip (i.e., plowing forces) and the (−) forces behind the tip increase to a greater extent than the other two types of forces. Thus, these two types of force, which arise from the hard-wall portion of the LJ potential, are the major contributors to the plowing friction.

Recent MD simulations have examined the nanotribology of alkylsilane SAMs using a finite-sized tip.[71] In these massively parallel simulations, an amorphous SiO_2 tip with radius of 10 nm was used to examine the mechanical and tribological properties of alkylsilane SAMs with chain lengths between C_{12} and C_{18}. The total friction as a function of load was linear, as it was when the tip was a flat plate, and showed little dependence on chain length. In those simulations, the tip radius was much larger than the thickness of the SAM. In this limit, the contact model of Reedy[57] is applicable. In MD simulations, as in experiment, contact between the tip and monolayer must be defined. Chandross *et al.*[66] defined contact to be the point where the distance between the tip and monolayer was smaller than 0.5 nm. When this definition of contact is used, the simulated contact area versus load predictions from the Reedy model more closely resembled the results from the MD simulations than the predictions from the DMT or JKR model.

In this work, it is the hydrogen atoms within the chains of the SAM that support the majority of the load on the tip at all loads because these atoms are in repulsive contact with the tip. In contrast, the carbon atoms that compose the backbones of the chains are separated from the tip by the hydrogen atoms. As a result, the majority of the forces acting on the carbon atoms are attractive in nature. At 0 nN, only a few hydrogen atoms directly below the tip are needed to account for the bulk of the repulsive interactions. As the load is increased, the fullerene penetrates into the monolayer. In this case, more hydrogen atoms underneath and at the edges of the tip are in repulsive contact with the tip [Fig. 8(b)]. The magnitude of the repulsive interactions is much larger than the magnitude of the attractive forces thus accounting for the net load on the tip. Because the actual force on each monolayer atom due to the tip is computed, the contact area could be defined as the number atoms with nonzero force. Using this definition of contact, the contact area is much larger than that predicted by DMT, JKR, or the Reedy model[91] in agreement with recent MD simulations of atomic-scale and nanoscale contacts.[50,81,82]

Despite the fact that continuum contact models underestimate the contact area, they have been successfully used to interpret AFM data.[8,18,41–51] The results presented here may shed insight into this apparent contradiction. Herein, it is shown that the majority of the load and friction at the sliding interface arises from interactions of the tip with a small number of atoms, while many more atoms contribute to the total load and total friction. At 10 nN of load, there are 1320 monolayer atoms with nonzero contact forces in the sliding direction. However, if load, and the contact area, were computed using the 32 atoms with the largest repelling (and attracting) forces, then ≈96% and ≈88% of the load and friction would be taken into account. If the contact area is computed using the 32 atoms with the largest force in the loading direction, then the results from the MD simulations more closely resemble the predictions from the Reedy model.[91] The fact that the interaction of a few atoms is responsible for the bulk of the load and the friction is important if one considers an AFM tip. Even if the size of the tip is well known, the number of atoms that contribute to the contact area may be less than what might be inferred from the tip radius. In addition, if the tip contains irregularities (i.e., is not perfectly smooth), these areas of the tip may contribute greatly to the interactions between the tip and the sample while only being a small geometric feature. In this case, a few SAM atoms might experience even greater forces than the maximum seen in this work.

ACKNOWLEDGMENTS

M.T.K., P.T.M., and J.A.H. acknowledge support from ONR under Contract No. N0001408WR20106. B.I.D. acknowledges ONR support, both directly and through the NRL. J.A.H. also acknowledges support from AFOSR under Contracts No. F1ATA08018G001 and No. F1ATA07351G001 as part of the Extreme Friction MURI.

[1] W. Unertl, J. Vac. Sci. Technol. A **17**, 1779 (1999).
[2] G. Gillies, C. Prestidge, and P. Attard, Langmuir **18**, 1674 (2002).
[3] U. Landman, W. D. Luedtke, N. A. Burnham, and R. J. Colton, Science **248**, 454 (1990).
[4] C. M. Mate, Wear **168**, 17 (1993).
[5] G. Germann, S. Cohen, G. Neubauer, G. McClelland, H. Seki, and D. Coulman, J. Appl. Phys. **73**, 163 (1993).
[6] P. Sheehan and C. Lieber, Science **272**, 1158 (1996).
[7] R. Carpick, N. Agrait, D. Ogletree, and M. Salmeron, J. Vac. Sci. Technol. B **14**, 1289 (1996).
[8] R. W. Carpick and M. Salmeron, Chem. Rev. (Washington, D.C.) **97**, 1163 (1997).
[9] A. Lio, D. H. Charych, and M. Salmeron, J. Phys. Chem. B **101**, 3800 (1997).
[10] S. S. Wong, H. Takano, and M. D. Porter, Anal. Chem. **70**, 5209

(1998).
[11] E. Barrena, C. Ocal, and M. Salmeron, J. Chem. Phys. **111**, 9797 (1999).
[12] E. Barrena, E. Palacios-Lidon, C. Munuera, X. Torrelles, S. Ferrer, U. Jonas, M. Salmeron, and C. Ocal, J. Am. Chem. Soc. **126**, 385 (2004).
[13] S. Lee, A. Puck, M. Graupe, R. Colorado, Jr., Y.-S. Shon, T. R. Lee, and S. S. Perry, Langmuir **17**, 7364 (2001).
[14] S. Lee, Y. S. Shon, R. Colorado, R. L. Guenard, T. R. Lee, and S. S. Perry, Langmuir **16**, 2220 (2000).
[15] J. E. Houston and H. I. Kim, Acc. Chem. Res. **35**, 547 (2002).
[16] J. E. Houston, C. M. Doelling, T. K. Vanderlick, Y. Hu, G. Scoles, I. Wenzl, and T. R. Lee, Langmuir **21**, 3926 (2005).
[17] S. Li, P. Cao, R. Colorado, Jr., X. Yan, I. Wenzl, O. E. Shmakova, M. Graupe, T. R. Lee, and S. S. Perry, Langmuir **21**, 933 (2005).
[18] I. Szlufarska, M. Chandross, and R. W. Carpick, J. Phys. D **41**, 123001 (2008).
[19] J. C. Love, L. A. Estroff, J. K. Kriebel, R. G. Nuzzo, and G. M. Whitesides, Chem. Rev. (Washington, D.C.) **105**, 1103 (2005).
[20] A. Ulman, Chem. Rev. (Washington, D.C.) **96**, 1533 (1996).
[21] U. Srinivasan, M. Houston, R. Howe, and R. Maboudian, J. Microelectromech. Syst. **7**, 252 (1998).
[22] M. Salmeron, Tribol. Lett. **10**, 69 (2001).
[23] N. M. Brewer, B. D. Beake, and G. J. Leggett, Langmuir **17**, 1970 (2001).
[24] E. W. van der Vegte, A. Subbotin, G. Hadziioannou, P. R. Ashton, and J. A. Preece, Langmuir **16**, 3249 (2000).
[25] X. Xiao, J. Hu, D. H. Charych, and M. Salmeron, Langmuir **12**, 235 (1996).
[26] E. Barrena, C. Ocal, and M. Salmeron, J. Chem. Phys. **113**, 2413 (2000).
[27] E. Flater, W. R. Ashurst, and R. Carpick, Langmuir **23**, 9242 (2007).
[28] H. I. Kim, T. Koini, T. R. Lee, and S. S. Perry, Langmuir **13**, 7192 (1997).
[29] H. I. Kim, M. Graupe, T. Oloba, O. Doini, S. Imaduddin, T. R. Lee, and S. S. Perry, Langmuir **15**, 3179 (1999).
[30] Y. Okabe, U. Akiba, and M. Fujihira, Appl. Surf. Sci. **157**, 398 (2000).
[31] E. Barrena, C. Ocal, and M. Salmeron, Surf. Sci. **482**, 1216 (2001).
[32] N. M. Brewer and G. J. Leggett, Langmuir **20**, 4109 (2004).
[33] A. Lio, C. Morant, D. F. Ogletree, and M. A. Salmeron, J. Phys. Chem. B **101**, 4767 (1997).
[34] E. Cooper and G. J. Leggett, Langmuir **15**, 1024 (1999).
[35] E. Barrena, S. Kopta, D. F. Ogletree, D. H. Charych, and M. Salmeron, Phys. Rev. Lett. **82**, 2880 (1999).
[36] W. Ashurst, C. Yau, C. Carraro, R. Maboudian, and M. Dugger, J. Microelectromech. Syst. **10**, 41 (2001).
[37] S. C. Clear and P. F. Nealey, Langmuir **17**, 720 (2001).
[38] X. Xiao, G. Lui, D. H. Charych, and M. Salmeron, Langmuir **11**, 1600 (1995).
[39] M. J. Brukman, G. O. Marco, T. D. Dunbar, L. D. Boardman, and R. W. Carpick, Langmuir **22**, 3988 (2006).
[40] K. Johnson, K. Kendall, and A. Roberts, Proc. R. Soc. London, Ser. A **324**, 301 (1971).
[41] M. A. Lantz, S. J. O'Shea, and M. E. Welland, Phys. Rev. B **56**, 15345 (1997).
[42] U. D. Schwarz, O. Zworner, P. Koster, and R. Wiesendanger, Phys. Rev. B **56**, 6987 (1997).
[43] M. Enachescu, R. J. A. van den Oetelaar, R. W. Carpick, D. F. Ogletree, C. F. J. Flipse, and M. Salmeron, Phys. Rev. Lett. **81**, 1877 (1998).
[44] J. D. Kiely and J. E. Houston, Phys. Rev. B **57**, 12588 (1998).
[45] M. Enachescu, R. van den Oetelaar, R. Carpick, D. Ogletree, C. Flipse, and M. Salmeron, Tribol. Lett. **7**, 73 (1999).
[46] E. Riedo, J. Chevrier, F. Comin, and H. Brune, Surf. Sci. **477**, 25 (2001).
[47] A. Socoliuc, R. Bennewitz, E. Gnecco, and E. Meyer, Phys. Rev. Lett. **92**, 134301 (2004).
[48] C. Ritter, M. Heyde, B. Stegemann, K. Rademann, and U. D. Schwarz, Phys. Rev. B **71**, 085405 (2005).
[49] B. Bhushan, J. N. Israelachvili, and U. Landman, Nature (London) **374**, 607 (1995).
[50] G. Gao, R. J. Cannara, R. W. Carpick, and J. A. Harrison, Langmuir **23**, 5394 (2007).
[51] M. J. Brukman, G. Gao, R. J. Nemanich, and J. A. Harrison, J. Phys. Chem. C **112**, 9358 (2008).
[52] R. Major, H. Kim, J. Houston, and X. Zhu, Tribol. Lett. **14**, 237 (2003).
[53] K. Johnson and I. Sridhar, J. Phys. D **34**, 683 (2001).
[54] K. Shull, Mater. Sci. Eng. R. **36**, 1 (2002).
[55] I. Sridhar, Z. Zheng, and K. Johnson, J. Phys. D **37**, 2886 (2004).
[56] D. Ebenstein and K. Wahl, J. Colloid Interface Sci. **298**, 652 (2006).
[57] E. Reedy, J. Mater. Res. **21**, 2660 (2006).
[58] Y.-Y. Lin, C.-F. Chang, and W.-T. Lee, Int. J. Solids Struct. **45**, 2220 (2008).
[59] M. Rutland, J. Tyrrell, and P. Attard, J. Adhes. Sci. Technol. **18**, 1199 (2004).
[60] P. Attard, J. Adhes. Sci. Technol. **16**, 753 (2002).
[61] M. Plunkett and M. Rutland, J. Adhes. Sci. Technol. **16**, 983 (2002).
[62] I. Sung and D. Kim, Appl. Phys. A: Mater. Sci. Process. **81**, 109 (2005).
[63] C. D. Wu, J. F. Lin, T. H. Fang, H. Y. Lin, and S. H. Chang, Appl. Phys. A: Mater. Sci. Process. **91**, 459 (2008).
[64] J. N. Glosli and G. M. McClelland, Phys. Rev. Lett. **70**, 1960 (1993).
[65] J. A. Harrison, G. T. Gao, R. J. Harrison, G. M. Chateauneuf, and P. T. Mikulski, in *Encyclopedia of Nanoscience and Nanotechnology*, edited by H. S. Nalwa (American Scientific, Los Angeles, 2004), Vol. 3, pp. 511–527.
[66] M. Chandross, G. S. Grest, and M. J. Stevens, Langmuir **18**, 8392 (2002).
[67] B. Park, M. Chandross, M. J. Stevens, and G. S. Grest, Langmuir **19**, 9239 (2003).
[68] B. Park, C. D. Lorenz, M. Chandross, M. J. Stevens, G. S. Grest, and O. A. Borodin, Langmuir **20**, 10007 (2004).
[69] M. Chandross, E. B. Webb, M. J. Stevens, G. S. Grest, and S. H. Garofalini, Phys. Rev. Lett. **93**, 166103 (2004).
[70] C. D. Lorenz, M. Chandross, G. S. Grest, M. J. Stevens, and E. B. Webb III, Langmuir **21**, 11744 (2005).
[71] M. Chandross, C. D. Lorenz, M. J. Stevens, and G. S. Grest, Langmuir **24**, 1240 (2008).
[72] A. B. Tutein, S. J. Stuart, and J. A. Harrison, J. Phys. Chem. B **103**, 11357 (1999).
[73] A. B. Tutein, S. J. Stuart, and J. A. Harrison, Langmuir **16**, 291

(2000).
[74] P. T. Mikulski and J. A. Harrison, J. Am. Chem. Soc. **123**, 6873 (2001).
[75] P. T. Mikulski and J. A. Harrison, Tribol. Lett. **10**, 29 (2001).
[76] G. M. Chateauneuf, P. T. Mikulski, G. Gao, and J. A. Harrison, J. Phys. Chem. B **108**, 16626 (2004).
[77] P. T. Mikulski, G. Gao, G. M. Chateauneuf, and J. A. Harrison, J. Chem. Phys. **122**, 024701 (2005).
[78] P. T. Mikulski, L. A. Herman, and J. A. Harrison, Langmuir **21**, 12197 (2005).
[79] J. A. Harrison, G. T. Gao, J. T. Schall, M. T. Knippenberg, and P. Mikulski, Philos. Trans. R. Soc. London, Ser. A **366**, 1469 (2008).
[80] J. A. Harrison, J. D. Schall, M. T. Knippenberg, G. T. Gao, and P. Mikulski, J. Phys.: Condens. Matter **20**, 354009 (2008).
[81] B. Luan and M. Robbins, Nature (London) **435**, 929 (2005).
[82] B. Q. Luan and M. O. Robbins, Phys. Rev. E **74**, 026111 (2006).
[83] H. J. C. Berendsen, J. P. M. Postma, W. F. van Gunsteren, A. DiNola, and J. R. Haak, J. Chem. Phys. **81**, 3684 (1984).
[84] B. Dunlap and R. Zope, Chem. Phys. Lett. **422**, 451 (2006).
[85] S. J. Stuart, A. B. Tutein, and J. A. Harrison, J. Chem. Phys. **112**, 6472 (2000).
[86] D. W. Brenner, O. A. Shenderova, J. A. Harrison, S. J. Stuart, B. Ni, and S. B. Sinnott, J. Phys.: Condens. Matter **14**, 783 (2002).
[87] L. Wenning and M. Müser, Europhys. Lett. **54**, 693 (2001).
[88] A. R. Burns, J. E. Houston, R. W. Carpick, and T. A. Michalske, Phys. Rev. Lett. **82**, 1181 (1999).
[89] U. Schwarz, O. Zworner, P. Koster, and R. Wiesendanger, J. Vac. Sci. Technol. B **15**, 1527 (1997).
[90] J. A. Harrison, S. J. Stuart, and A. B. Tutein, in *Interfacial Properties on the Submicron Scale*, ACS Symposium Series Vol. 781, edited by J. Frommer and R. M. Overney (American Chemical Society, Washington, DC, 2001), pp. 216–229.
[91] M. T. Knippenberg, P. T. Mikulski, B. I. Dunlap, and J. A. Harrison (unpublished).